Structural optimization of uniaxial symmetry non-circular bolt clearance hole on turbine disk

Chen Qiuren, Guo Haiding *, Zhang Chao, Liu Xiaogang

Jiangsu Province Key Laboratory of Aerospace Power System, Nanjing University of Aeronautics and Astronautics, Nanjing 210016, China

Abstract This study proposes a parameterized model of a uniaxial symmetry non-circular hole, to improve conventional circular bolt clearance holes on turbine disks. The profile of the model consists of eight smoothly connected arcs, the radiuses of which are determined by 5 design variables. By changing the design variables, the profile of the non-circular hole can be transformed to accommodate different load ratios, thereby improving the stress concentration of the area near the hole and that of the turbine disk. The uniaxial symmetry non-circular hole is optimized based on finite element method (FEM), in which the maximum first principal stress is taken as the objective function. After optimization, the stress concentration is evidently relieved; the maximum first principal stress and the maximum von Mises stress on the critical area are reduced by 30.39% and 25.34% respectively, showing that the uniaxial symmetry non-circular hole is capable of reducing the stress level of bolt clearance holes on the turbine disk.

1. Introduction

Bolt clearance holes, pin holes and vent holes on turbine disks or compressor disks are critical regions for which life certification are necessary. The main loads associated with these regions are centrifugal structural forces and thermal loads. Generally, there exists a high level stress concentration around these areas, which may seriously reduce the fatigue resistance of the disk.[1] Some processes like chamfering, polishing and surface treatments are applied to handle it. However, even with all these technical processes, we cannot effectively decrease the stress concentration around these areas which crucially influences the thermo-mechanical integrity of turbine disks and the durability of gas turbine engines as well.[2–5]

One effective approach to lessen the stress concentration is to change the profile of the hole. The non-circular hole can be a feasible option. The non-circular hole was firstly applied to the design of tunnel profiles to decrease stress concentration.[6,7] Chen et al.[8] proposed a 3-variable turbine disk non-circular hole, the profile of which is symmetry to both X and Y axes and can fit the stress state by changing the design variables. This 3-variable non-circular hole was proved to be effective for reducing stress concentration on the edge of the bolt clearance hole after optimization.

* Corresponding author. Tel.: +86 25 84892202 2102.

E-mail addresses: nuaacqr@126.com (Q. Chen), ghd@nuaa.edu.cn (H. Guo), zcnuaa@126.com (C. Zhang), elflxg@163.com (X. Liu).
Peer review under responsibility of Editorial Committee of CJA.

When applied as bolt clearance holes on the turbine disk, non-circular holes with approximate square profiles are especially beneficial for inserting the widely used anchor locking nuts on aero engine disks. And the anchor locking nuts are able to lock the bolts by their square external profiles, preventing the bolts from rotating in the bolt holes. However, little information for the non-circular hole design of aero engine disks has been reported up till now. To reduce stress concentration, the profile of a non-circular hole should be smooth and continuous. Moreover, when bolt clearance holes are considered, the fit tolerance of holes and bolts should also be guaranteed. To balance machining cost and quality, the minimum radius of the profile should be determined by the geometry of standard cutting tools.

The present paper proposes a mathematical model of the uniaxial symmetry non-circular hole, whose profile consists of eight smoothly connected arcs. An FEM-based optimization model for the hole is proposed, and the superiority of uniaxial symmetry non-circular hole over the circular hole is then proved. In the optimization, a high pressure turbine disk with such a non-circular bolt clearance hole on the collar is modeled and analyzed. The maximum first principal stress around the critical area is obtained as the optimal objective in the optimization. The results obtained are discussed in terms of the maximum stress/strain level on the inner surface and the stress distribution along the edge of the holes.

2. Geometry modeling

2.1. Basic agreement

The uniaxial symmetry non-circular hole is symmetrical to Y axis, constrained in a rectangle ($2b \times 2a$). Variables a and b are defined as the lengths of vertical semi-axis and horizontal semi-axis respectively (see Fig. 1).

As shown in Fig. 1, the profile of the uniaxial symmetry non-circular hole consists of main arc A on the top (radius $r = R_1$), main arc B on the bottom ($r = R_2$), two symmetry lateral main arcs C on either side ($r = R_3$), two symmetry upper transition arcs D ($r = R_4$) and two symmetry bottom transition arcs E ($r = R_5$). R_1, R_2, R_3, R_4 and R_5 are chosen as independent design variables for subsequent optimization.

When positional machining errors of the bolt clearance holes are concerned, it is much more difficult to control the circumferential machining error accumulation than the radial machining errors on the turbine disk. In consideration of this issue, we suggest that the horizontal semi-axis b, which is independent of the vertical semi-axis a, be larger than a. This is beneficial for tolerating larger circumferential machining errors of the hole.
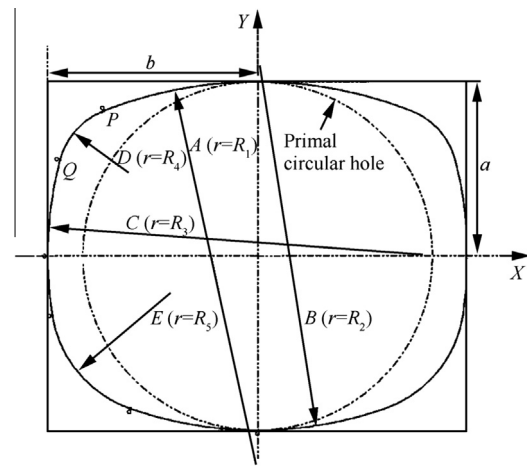

Fig. 1 Geometry model of uniaxial symmetry non-circular hole.

2.2. Constraint functions

The uniaxial symmetry non-circular hole discussed here is symmetrical to Y axis; therefore, only the left half of the profile is studied in the paper. In this case, the value ranges of the radiuses must ensure that the transition arcs are able to connect with the main arcs (i.e. R_1 to R_4 and R_2 to R_5) smoothly. According to Ref.[9], R_1, R_2 and R_3 should satisfy

$$\begin{cases} R_1 > \dfrac{a^2 + b^2}{2a} \\ R_2 > \dfrac{a^2 + b^2}{2a} \\ R_3 > \dfrac{a^2 + b^2}{2b} \end{cases} \tag{1}$$

The boundaries of transition arcs C and D can be expressed by

$$\begin{cases} R_4 < \dfrac{b^2 + m^2 - R_1^2}{2(b - R_1)} \\ R_5 < \dfrac{b^2 + m'^2 - R_2^2}{2(b - R_2)} \end{cases} \tag{2}$$

where $m = R_1 - a$, $m' = R_2 - a$.

Based on the connection conditions of the arcs, the center coordinates of the transition arc D can be expressed by Eq. (3), which ensures the smooth connection among arcs R_1, R_4 and R_3. In addition, in the third quadrant, the center coordinates of the transition arc E are expressed by Eq. (4).

$$\begin{cases} x_4 = \dfrac{-en - 2nm^2 - \sqrt{-e^2m^2 + 4em^2n^2 + 4j^2m^2n^2 - 4m^2n^4 + 4j^2m^4}}{2(m^2 + n^2)} \\ y_4 = \dfrac{em - 2mn^2 + \sqrt{-e^2n^2 - 4em^2n^2 + 4i^2m^2n^2 - 4m^4n^2 + 4i^2n^4}}{2(m^2 + n^2)} \end{cases} \tag{3}$$

$$\begin{cases} x_5 = \dfrac{-e'n' - 2n'm'^2 - \sqrt{-e'^2m'^2 + 4e'm'^2n'^2 + 4j'^2m'^2n'^2 - 4m'^2n'^4 + 4j'^2m'^4}}{2(m'^2 + n'^2)} \\ y_5 = -\dfrac{e'm' - 2m'n'^2 + \sqrt{-e'^2n'^2 - 4e'm'^2n'^2 + 4i'^2m'^2n'^2 - 4m'^4n'^2 + 4i'^2n'^4}}{2(m'^2 + n'^2)} \end{cases} \tag{4}$$

where $n = a - R_2$, $i = R_1 - R_3$, $j = R_2 - R_3$, $e = i^2 - j^2 + n^2 - m^2$, $n' = b - R_3$, $i' = R_2 - R_5$, $j' = R_3 - R_5$, $e' = i'^2 - j'^2 + n'^2 - m'^2$.

At the same time, coordinates of the tangent point P (see Fig. 1) between arc D and arc A can be expressed by

$$\begin{cases} x_P = -\dfrac{R_1}{g} \\ y_P = \dfrac{-mR_1 - R_1 y_3 - gmx_3}{gx_3} \end{cases} \tag{5}$$

where x_3 and y_3 are the center coordinates of the lateral main arc R_3, and g is defined by

$$g = \sqrt{1 + \left(\frac{y_3 + m}{x_3}\right)^2} \tag{6}$$

The coordinates of tangent point Q (see Fig. 1) between arc D and arc C are expressed by

$$\begin{cases} x_Q = \dfrac{-n - f^2 n - \sqrt{R_2^2 + f^2 R_2^2}}{1 + f^2} \\ y_Q = -\dfrac{f\sqrt{(1 + f^2)R_2^2}}{1 + f^2} \end{cases} \tag{7}$$

where f is defined by

$$f = \frac{y_3}{x_3 + n} \tag{8}$$

The center coordinates of the transition arcs must satisfy Eq. (3) and Eq. (4) so that the connections could be tangent. In other quadrants, the arcs connect with each other in a similar geometric relationship.

2.3. Discussion of model

When R_2 and R_5 are equal to R_1 and R_4 respectively, the uniaxial symmetry non-circular hole degenerates into a biaxial symmetry non-circular hole which is symmetry to both X axis and Y axis. When b and values of all design variables (R_1 to R_5) are equal to a, the profile of the hole degenerates into the original circular bolt clearance hole.

Compared with the biaxial symmetry non-circular hole, a uniaxial symmetry non-circular hole has two more design variables, which makes its profile more flexible to accommodate the complex stress distribution on the turbine disks.

3. Optimization example on a turbine disk collar

3.1. FEM-based structural analysis

In this paper, a high pressure turbine (HPT) disk is employed as an example to validate the superiority of the proposed uniaxial symmetry non-circular hole.

In the analysis, the heat load is not considered, as the thermal stress gradient on the turbine collar presents negligible influence to the maximum stress and stress/strain distribution on critical areas of the hole.[9] The structure platforms and blades are neglected and substituted by an equivalent centrifugal load applied on the disk rim. Fig. 2 shows the 1/48 sector model of the HTP disk.
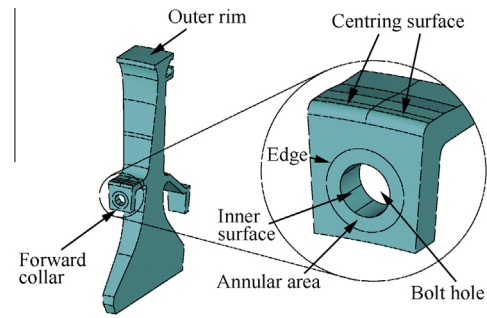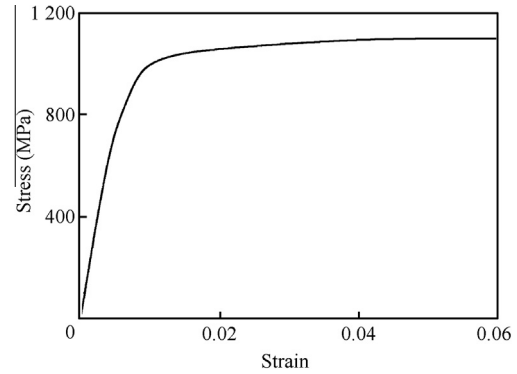

Fig. 2   1/48 sector of HTP disk.

Fig. 3   Stress vs strain curve of GH4169 in 500 °C.

The torque load is applied to the front surface of the forward collar before it is transformed into a circumference stress of 2.7 kN for each sector. The extrusion force on the centring surface of the collar is simplified to a radial pressure (132.6 MN for each sector).[10] The rotation speed of the turbine is 14400 r/min. The finite element mesh is particularly refined on the annular area around the hole to guarantee accurate results. The material employed is a Ni-based high temperature alloy designated 'GH4169', and the constitutive relationship of the material in 500 °C is shown in Fig. 3.

3.2. Optimization model

It is recognized that, for the fatigue life of axial bolt clearance holes on turbine disks, the tangential stress on the edge of the hole is the main driving force of crack propagation.[11] The tangential stress in this circumstance is approximate to the first principal stress on the inner surface of the axial bolt clearance holes. For this reason, the maximum first principal stress $\sigma_{1\max}$ on the inner surface of the non-circular hole is chosen as the objective function of the optimization.

In order to assess the optimization results, we define K_1 as the decline ratio of $\sigma_{1\max}$ on the inner surface of the hole, as shown in Eq. (9).

$$K_1 = \frac{\sigma_{1\max} - \sigma_{1\max\,0}}{\sigma_{1\max 0}} \times 100\% \tag{9}$$

where $\sigma_{1\max}$ and $\sigma_{1\max\,0}$ represent the maximum first principal stress of the optimized non-circular hole and the primal circular hole ($r = a$) respectively. The optimization model can be expressed by
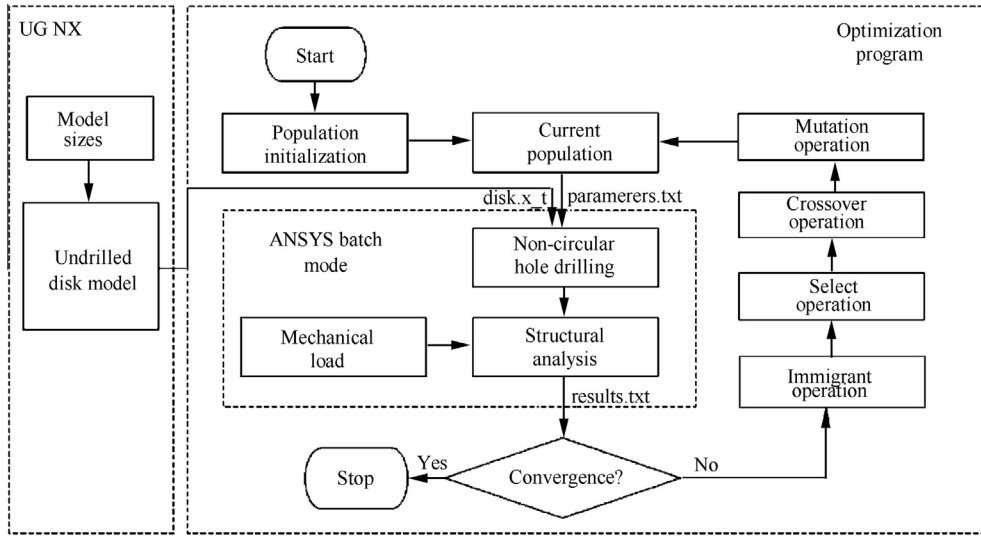
Fig. 4 Integration of optimization process.

$$\begin{cases} \min\ f(R_i) = \sigma_{1\max}\ (i = 1, 2, 3, 4, 5) \\ \text{s.t.}\ R_1 > \dfrac{a^2 + b^2}{2a} \\ R_2 > \dfrac{a^2 + b^2}{2a} \\ R_3 > \dfrac{a^2 + b^2}{2b} \\ \dfrac{b^2 + m^2 - R_1^2}{2(b - R_1)} > R_4 > R_{\min} \\ \dfrac{b^2 + m'^2 - R_1^2}{2(b - R_1)} > R_5 > R_{\min} \end{cases} \quad (10)$$

where $R_{\min}$ represents the minimum acceptable radius for cutting tools. According to Ref.[12], $R_{\min}$ is set as 1 mm.

3.3. Optimization scheme

The present study employs a Visual Basic program coded with elite-preservation adaptive genetic algorithm in the optimization procedure, by which the global optimum for the uniaxial symmetry non-circular hole can be ensured.[13–15]

The turbine disk without holes is modeled in UG NX prior to the computation. The optimization program is integrated with ANSYS, which is used to analyze the model and output the results into the optimization program.[16–20] The flowchart of the optimization process for the non-circular hole is demonstrated in Fig. 4.

4. Results and discussion

In the optimization, vertical semi-axis a and horizontal semi-axis b are set as 5.00 mm and 5.25 mm respectively, according to the design standard series of bolt clearance holes. The population quantity and the maximum iteration number are set as 20 and 35 respectively. In order to compare the effectiveness of uniaxial symmetry non-circular hole and biaxial symmetry non-circular hole, we also optimize a biaxial symmetry non-circular hole. The optimization results are tabulated in Table 1.

As shown in Table 1, compared with circular holes, the radiuses of the main arcs, especially R_3 of the optimum non-circular holes, are much larger (for both biaxial symmetry and uniaxial symmetry). And this makes the profiles of the non-circular holes much flatter. The maximum first principal stress of the optimized non-circular hole (uniaxial symmetry) is 252.90 MPa and 258.39 MPa lower than those of the 5.00 mm and 5.25 mm circular holes respectively. It is reasonable to deduce that, larger main arc radiuses are beneficial for decreasing the stress and strain on the inner surface of the bolt clearance hole. In Fig. 5, the maximum first principal stress distribution of collars (1/48 sectors) with a circular hole ($r = a = 5.00$ mm) is demonstrated.

As shown in Fig. 5, the maximum first principal stress point of the circular hole is located at the bottom of the inner surface of the hole, and the high stress area converges in a small area. The stress distributions of optimal uniaxial symmetry non-circular hole and biaxial symmetry non-circular hole are shown in Fig. 6 and Fig. 7 respectively. We can see that the maximum first principal stress point is located at the bottom or top of the hole. The high stress area has moderate expansion, while the value of the maximum stress decreases obviously (see Fig. 6).

According to Table 2, the maximum von Mises stress on the inner surface of the optimized uniaxial symmetry non-circular hole is 187.95 MPa lower than that of the circular hole ($r = a$).

Table 1 Optimization results with $\sigma_{1\max}$ based objective function.

Hole type		R_1 (mm)	R_2 (mm)	R_3 (mm)	R_4 (mm)	R_5 (mm)	$\sigma_{1\max}$ (MPa)
Circular	$r = a = 5.00$ mm	5.00	5.00	5.00	5.00	5.00	832.25
	$r = b = 5.25$ mm	5.25	5.25	5.25	5.25	5.25	837.74
Optimized non-circular	Biaxial symmetry	29.30	29.30	75.80	3.10	3.10	621.28
	Uniaxial symmetry	21.40	32.70	62.50	3.30	1.60	579.35

σ₁ (MPa) −45.4 62.5 171 278 386 494 602 710 818 926   σ₁ (MPa) −45.4 62.5 171 278 386 494 602 710 818 926

(a) Front view   (b) Oblique view
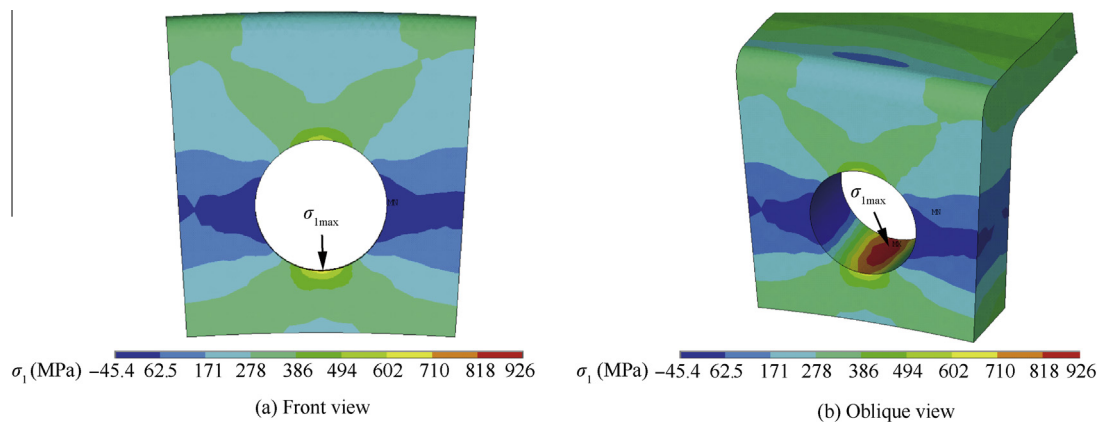
Fig. 5   Stress distribution of circular bolt clearance hole ($r = 5.00$ mm).

σ₁ (MPa) −29 49.2 127 206 284 362 440 518 597 675   σ₁ (MPa) −29 49.2 127 206 284 362 440 518 597 675

(a) Front view   (b) Oblique view
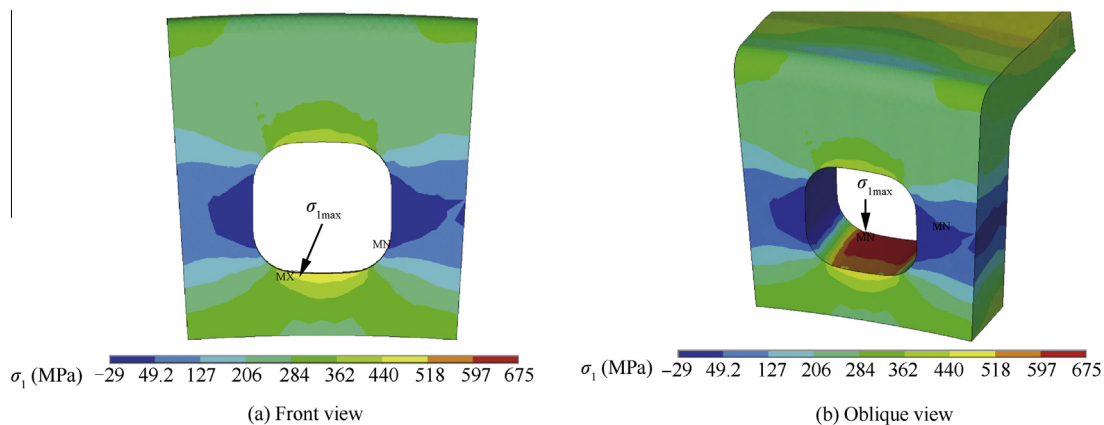
Fig. 6   Stress distribution of optimized biaxial symmetry non-circular bolt clearance hole.

σ₁ (MPa) −28 44.9 118 191 264 337 410 482 555 628   σ₁ (MPa) −24.5 47.8 120 193 265 337 410 482 554 627

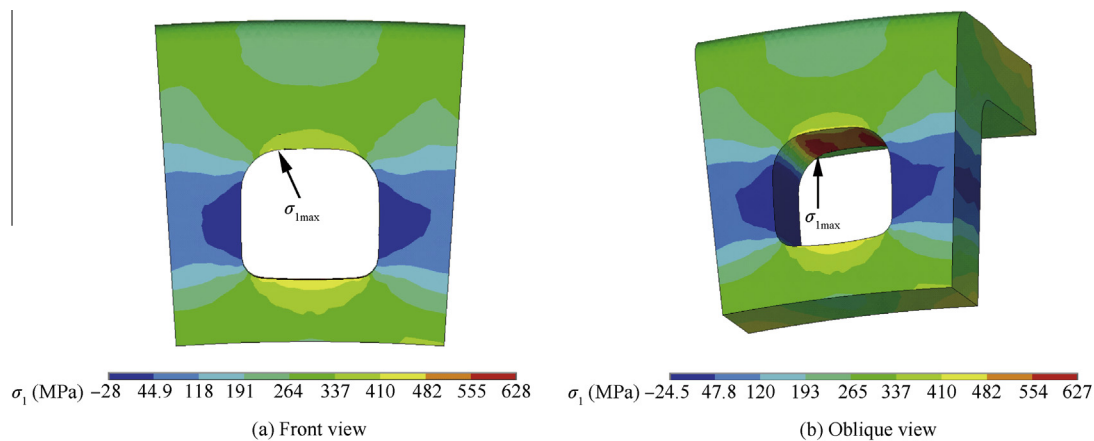(a) Front view   (b) Oblique view

Fig. 7   Stress distribution of the optimized uniaxial symmetry non-circular bolt clearance hole.

Table 2   Stress and strain values of circular holes and non-circular holes.

Hole types		σ_{eqvmax} (MPa)	$\varepsilon_{1\max}$ (10^{-3})	$\varepsilon_{\text{eqvmax}}$ (10^{-3})	K_{t}	K_1 (%)
Circular	$r = a = 5.00$ mm	767.31	5.21	7.02	2.39	N/A
	$r = b = 5.25$ mm	760.12	5.04	6.83	2.37	N/A
Optimized non-circular	Biaxial symmetry	598.45	3.79	5.16	1.87	25.34
	Uniaxial symmetry	579.36	3.62	4.95	1.80	30.39

(a) Start-stop angle
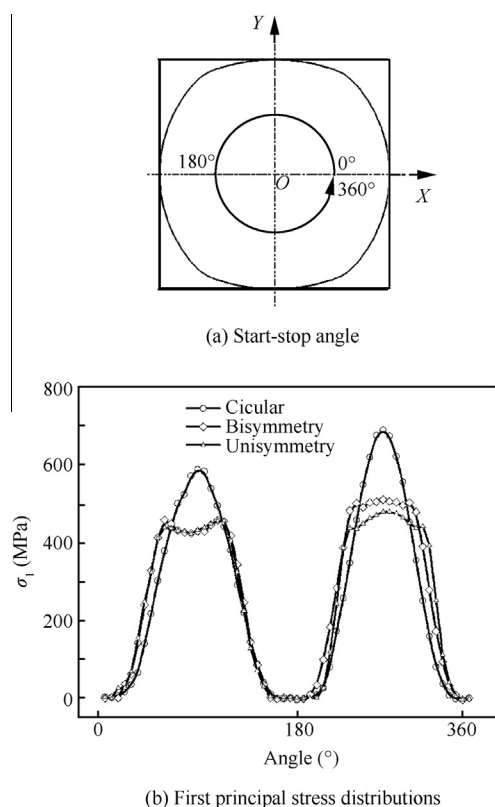

(b) First principal stress distributions

Fig. 8 First principal stress distribution along edge of the holes.

The total mechanical strain also obtains a notable decrease after optimization. More precisely, with regard to the optimal uniaxial symmetry non-circular hole, the maximum first principal strain and the maximum von Mises strain decrease by 30.51% and 29.48% respectively. The stress concentration factor K_t decreases by over 24.68%, from 2.39 to 1.80.

Table 2 also shows that the stress/strain results of the optimal non-circular hole is superior to circular holes whether the radius is b or a. In addition, the decrease of the stress/strain of the uniaxial symmetry non-circular hole is obviously greater than that of the biaxial symmetry non-circular hole, proving the superiority of uniaxial symmetry non-circular holes over biaxial symmetry non-circular holes.

In order to study the stress variation along the edge precisely, the first principal stress on the edge of the holes is obtained (on the nodes along the edge) and plotted in Fig. 8.

As shown in Fig. 8, the first principal stress of the circular hole ($r = 5.00$ mm) reaches its second highest value at the top of the hole. The difference of the stress concentration level between the top and the bottom is due to the variation of the nominal stress along the radial direction on the disk collar. With regard to the optimal bisymmetry non-circular hole, the peak values at the top and the bottom of the edge decrease by around 150 MPa and 200 MPa respectively, in comparison with the primal circular hole. Similar trends happen on the optimal uniaxial symmetry non-circular hole, but the stress level at the bottom of the edge is approximately 40 MPa lower than the bisymmetry non-circular hole. The uniaxial symmetry non-circular hole holds two more design variables, which makes it possible to change its profile under the X axis independently to accommodate the stress variation along the radial direction of the disk.

5. Conclusions

This paper proposes a uniaxial symmetry bolt clearance hole which consists of eight smoothly connected arcs. The profile of the uniaxial symmetry hole can accommodate different load conditions to improve stress concentration. The non-circular hole with an approximate rectangular profile is proved to be beneficial for decreasing the stress concentration of the clearance hole on the turbine disk.

The present study defines the maximum first principal stress on the inner surface of the hole as the objective function, and employs an elite-preservation adaptive genetic algorithm combined with FEM to find the optimal parameters for the non-circular holes. With the present work, the following conclusions can be drawn:

(1) The proposed geometry model guarantees the smooth connection among the arcs of the uniaxial symmetry non-circular hole. The profile of the hole is determined by semi-axis lengths a, b, as well as the 5 design variables. The geometric transformation of the hole presents significant influence on the stress distribution and maximum first principal stress on the edge of the non-circular hole.
(2) By using the maximum first principal stress as the objective function, the stress concentration factor K_t on the inner surface of the uniaxial symmetry non-circular hole can be reduced by over 24% after optimization. Moreover, the high stress on the top and bottom of the edge decreases obviously, which can effectively improve the fatigue resistance of the structure.
(3) The uniaxial symmetry non-circular hole is more capable of accommodating the stress variation along the radial direction on the turbine than the biaxial symmetry non-circular hole, since it can change its profile under the X axis independently.

It should be noted that, the connection between the arcs must be smooth, and no scratch is allowed. Additionally, some modifications can also be made on the design variables in consideration of the limitation of cutting tools, the cost and the convenience of technical process.

References

1. Li W, Dong LW, Cai XH, Zhao FX, Liu D. Structure analysis and life evaluation of the pin holes in a turbine disk of a type of aero-engine. *J Aerosp Power* 2009;**24**(8):699–706 [Chinese].
2. Lu S, Huang QQ. New method for damage tolerance analysis of turbine disk and its application. *J Aerosp Power* 2002;**17**(1):87–92 [Chinese].
3. Shi YJ, Wang M. Analysis on shear behavior of high-strength bolts connection. *Int J Steel Struct* 2011;**11**(2):203–13 [Chinese].
4. Pedersen NL. Optimization of bolt thread stress concentrations. *J Arch Appl Mech* 2013;**83**(1):1–14.

5. Gao Y, Bai GC, Zhang YL. Reliability analysis of multi-axial low cycle fatigue life for turbine disk. *Acta Aeronaut et Astronaut Sin* 2009;**30**(9):678–782 [Chinese].

6. Bjorkman GS, Richards R. Harmonic hole for non constant field. *J ASME J Appl Mech* 1979;**47**(2):573–6.

7. Dhir SK. Optimization in a class of hole shapes in plate structures. *J ASME J Appl Mech* 1981;**48**:905–8.

8. Chen QR, Guo HD, Liu XG. Modeling and optimization for the structure of biaxial symmetry non-circular hole of the turbine disk. *J Aerosp Power* 2013;**28**(6):250–6 [Chinese].

9. Chen QR. Structure design and optimization of non-circular hole on turbine disks [dissertation]. Nanjing: Nanjing University of Aeronautics and Astronautics; 2013 [Chinese].

10. Zhang C, Guo HD, Chen QR. Nonlinear FEM analysis of the contact stress on interference fitting surfaces for turbine disk based on non-circular hole. In: Sun W, Li M, Jiang J, editors. *Proceedings of the 9th China CAE annual conference*; 2013 July 27–28; Huangshan, Anhui. Beijing: CIBTC; 2013.p.215-7 [Chinese].

11. Gong M, Zhao JH, Dong BH, Wang XF, Li CZ. Initiation and propagation of fatigue crack in edge region of hole in a sheet with central hole. *Acta Aeronaut et Astronaut Sin* 2002;**23**(3):02–5 [Chinese].

12. Wei X. Study on machining process of shaped hole in Ni-base super-heat-resistant alloy work pieces. *Tool Eng* 2002;**36**(6):9–23 [Chinese].

13. Cheng H, Yang SX. Genetic algorithms with immigrant schemes for dynamic multicast problems in mobile adhoc networks. *J Eng Appl Artif Intell* 2010;**23**(5):806–19.

14. Zafer B. Adaptive genetic algorithms applied to dynamic multi-objective problems. *J Appl Soft Comput* 2007;**7**(3):791–9.

15. Srinivasa KG, Venugopal KR, Patnaik LM. A self-adaptive migration model genetic algorithm for data mining applications. *J Inf Sci* 2007;**177**(20):4295–313.

16. Gao JH, Wen WD, Cui HT. Optimal design for temperature and structure of the float-wall of flame tube. *J Aerosp Power* 2012;**27**(3):88–94 [Chinese].

17. Gao JH, Wen WD, Cui HT. Genetic algorithm model-based optimization for float-wall with thermal-structural coupled. *J Aerosp Power* 2012;**27**(1):2–7 [Chinese].

18. Sun MH, Cui HT, Wen WD. Topology optimization of continuum structure under multiple constraints using genetic algorithm with elitist strategy. *J Aerosp Power* 2006;**21**(4):732–7 [Chinese].

19. Yang SX, Tinós R. A hybrid immigrants scheme for genetic algorithms in dynamic environments. *Int J Autom Comput* 2007;**4**(3):243–54.

20. Tinós R, Yang SX. A self-organizing random immigrants genetic algorithm for dynamic optimization problems. *Genet Programming Evolvable Mach* 2007;**8**(3):255–86.

Chen Qiuren received the B.S. and M.S. degrees in aeronautic engine engineering from Nanjing University of Aeronautics and Astronautics in 2010 and 2013 respectively. Now he is a Ph.D. student in mechanical engineering. His area of research includes structural optimization and fatigue modeling.

Guo Haiding is a professor and Ph.D. supervisor at College of Energy and Power Engineering, Nanjing University of Aeronautics and Astronautics, Nanjing, China. His current research interests are fatigue damage modeling and life prediction of welded material, and artificial structural optimization techniques.

Zhang Chao is a graduate student and an assistant engineer. His area of research includes structural strength and vibration, and maintenance engineering of aero engines.

Liu Xiaogang is an associate professor at College of Energy and Power Engineering, Nanjing University of Aeronautics and Astronautics, Nanjing, China. His current research interests are structural strength and fatigue fracture.